Sciencexpress Report

Nondestructive Optical Measurements of a Single Electron Spin in a Quantum Dot

J. Berezovsky, M. H. Mikkelsen, O. Gywat, N. G. Stoltz, L. A. Coldren, D. D. Awschalom*

Center for Spintronics and Quantum Computation, University of California, Santa Barbara, CA 93106, USA.

*To whom correspondence should be addressed. E-mail: awsch@physics.ucsb.edu

Kerr rotation measurements on a single electron spin confined in a charge-tunable semiconductor quantum dot demonstrate a means to directly probe the spin off-resonance, thus minimally disturbing the system. Energy-resolved magneto-optical spectra reveal information about the optically-oriented spin polarization and the transverse spin lifetime of the electron as a function of the charging of the dot. These results represent progress towards the manipulation and coupling of single spins and photons for quantum information processing.

The prospect of quantum computation in conventional material systems has spurred much research into the physics of carrier spins in semiconductor quantum dots (QDs) (*1*). An important element necessary for spin-based quantum computing is the read-out of the qubit spin state. Previously demonstrated schemes for single spin read-out in a quantum dot include optical measurements, such as photoluminescence (PL) polarization (*2*, *3*) or polarization-dependent absorption (*4*–*6*). Single spins can also be read out electrically by measuring the spin-dependent probability for an electron to tunnel out of the dot (*7*). However, these methods are destructive, in that they either remove the spin from the dot, or drive transitions in the system with a resonant optical field. In contrast, we describe measurements of a single electron spin using Kerr rotation (KR) in which the spin state is probed non-resonantly, thus minimally disturbing the system. This effective spin-photon interaction has been shown to allow for Schrödinger's cat-type measurements to probe quantum effects such as measurement-induced decoherence and spin squeezing (*8*, *9*) as well as the implementation of quantum information protocols involving spin-photon entanglement (*10*) and optically-mediated spin-spin entanglement (*11*–*13*).

In the present work, the electrons are confined to a single charge-tunable QD formed by monolayer fluctuations at the interfaces of a GaAs quantum well (QW). The QD layer is centered within an optical microcavity with a resonance chosen to enhance the interaction of the optical field with the QD at energies well below the lowest interband transition. By applying a transverse magnetic field, the electron spins can be depolarized in a Hanle-type measurement, thereby yielding information about the spin lifetime.

The magneto-optical Kerr effect results in a rotation of the plane of polarization of linearly polarized light with energy E upon reflection off the sample, and is analogous to the Faraday effect for transmitted light. For both effects, the rotation angle is determined by the difference of the dynamic dielectric response functions for σ^+ and σ^- circularly polarized light, which are proportional to the interband momentum matrix elements, $\left\langle \psi_c \middle| \hat{p}_x \pm i\hat{p}_y \middle| \psi_v \right\rangle$, where ψ_c (ψ_v) is a conduction (valence) band state (*14*, *15*). Due to the microcavity, both reflection and transmission contribute to the measured polarization rotation. For simplicity, we refer only to KR. For a single conduction-band energy level in a QD containing a spin-up electron in a state $\left|\psi_\uparrow\right\rangle$, optical transitions to the spin-up state are Pauli-blocked, and the KR angle is then given by

$$\theta_K(E) = CE \sum_{\alpha=\pm1;v} \alpha \left|\left\langle \psi_\downarrow \middle| \hat{p}_x + \alpha i\hat{p}_y \middle| \psi_v \right\rangle\right|^2 \frac{E - E_{0,v}}{\left(E - E_{0,v}\right)^2 + \Gamma_v^{\,2}} \qquad (1)$$

where C is a constant, and $E_{0,v}$ and Γ_v are the energy and linewidth of the transition involving the valence band state $\left|\psi_v\right\rangle$, respectively. We focus on a single transition in the sum in Eq. 1 and drop the index v. For $\Gamma << |\Delta| << E$, where $\Delta = E - E_0$, we note that $\theta_K \sim \Delta^{-1}$, which decays slower than the absorption line, $\sim\Delta^{-2}$ (*15*, *16*). Therefore, for a suitable detuning, Δ, KR can be detected while photon absorption is strongly suppressed.

The sample structure (Fig. 1A) is grown by molecular beam epitaxy and consists of a single 4.2-nm GaAs QW in the center of a planar $\mathrm{Al}_{0.3}\mathrm{Ga}_{0.7}\mathrm{As}$ λ-cavity (*34*). The reflectivity of the sample at 10 K (Fig. 1D) shows a cavity resonance centered at 763.6 nm (1.624 eV) with a Q-factor of 120. The probe light effectively interacts with the spin many times as it is reflected back and forth within the cavity. As a result, the polarization rotation described by Eq. 1 occurs repeatedly, enhancing the small, single spin KR angle (*19*). Based on previous measurements with similar cavities (*20*, *21*), we expect the KR at the peak of the cavity resonance to be enhanced by a factor of ~15.

The band profile for our structure (*34*), calculated with a 1-D self-consistent Poisson-Schrödinger solver, is shown in Fig. 1B. By applying a bias across the structure, the conduction band minimum in the QW can be made to plunge beneath the Fermi level, charging first the QDs, then the well itself (*22*, *23*). The onset of this charging occurs around 0.5V (Fig. 1C) according to the band-structure calculation.

A cw Ti:Sapphire laser (1.654-1.662 eV) is focused through a microscope objective (spot size ~ 2μm) on the sample at T = 10 K to excite electron-hole pairs into the continuum of states in the QW. The carriers then relax into the QDs, and the subsequent PL is collected through the same objective, dispersed in a spectrometer, and detected by a liquid-nitrogen-cooled CCD. In a typical single dot PL spectrum as a function of the applied bias (Fig. 2A), the sharp features (linewidth ~100 μeV) are characteristic of single-dot PL (*18*), demonstrating the presence of only one QD within the laser focus. Above 0.5V a single line is observed at 1.6297 eV which is attributed to recombination from the negatively-charged exciton (trion, or X^-) state. Below 0.5V this line persists faintly, and a bright line appears 3.6 meV higher in energy due to the neutral exciton (X^0) transition. The presence of the X^- line at $V_b < 0.5$ V implies that occasionally a single electron is trapped in the dot, forming an X^- when binding to an electron and a hole. In addition, a faint line at 1.6292 eV is visible from radiative decay of the biexciton (XX). These assignments of the observed lines are consistent with measurements on similar structures (*2*, *23*), and are further supported by the linear dependence of the X^- and X^0 lines, and the quadratic dependence of the XX line on the excitation intensity. Figure 3C illustrates these three optical transitions. In this QD we see no evidence of a positively charged exciton.

With circularly polarized excitation, spin polarized electrons and heavy holes can be pumped into the QD due to the optical selection rules of the GaAs QW (*2*, *24*). For the purposes of this discussion, spin polarization parallel to the optically injected electron spin polarization will be referred to as “spin-up”, and the opposite spin as “spin-down”. Information about the spin polarization in the QD can be gained from the polarization of the PL (*2*). The circular polarization of the PL is determined by switching the helicity of the pump from σ^+ to σ^- and measuring the intensity of the σ^+-polarized PL, (I^+ and I^-, respectively). The polarization is then defined as $P = (I^+ - I^-)/(I^+ + I^-)$ and is shown for the X^0 and X^- lines in Fig. 2B, in agreement with earlier results (*2*, *23*).

The polarization of the X^- line is determined by the hole spin, as the two electrons in the trion form a spin-singlet state. In the uncharged regime ($V_b < 0.5$ V), the negative polarization of the X^- PL indicates that the heavy hole undergoes a spin-flip before recombination in most cases. Hole spin-flips may occur either during energy relaxation in the QW (*25*) or by an exchange-mediated electron-hole spin-flip (*26*). Regardless of the hole spin-flip process, after the recombination of the X^-, the electron left in the QD is polarized in the spin-up direction. In this way, both optical injection and trion recombination serve to pump lone spin-up electrons into the QD.

When the dot is initially charged near $V_b = 0.5$ V, the now dominant X^- line remains negatively polarized, resulting in continued pumping of the spin-up state. As the electron density in the QW increases with higher applied bias, the X^- polarization becomes positive, as has been previously observed (*2*, *23*).

In a transverse applied magnetic field, the electron spins precess, depolarizing the PL. The hole spins do not precess (*27*) because the heavy and light hole states are split (by ~20 meV in our sample (*28*)), leading to an effective heavy-hole g factor of zero in the plane of the QW. Hanle measurements on this dot are summarized in Fig. 2C. In the charged regime, at $V_b = 0.9$V, no depolarization of the X^- PL is observed, as expected for polarization due to the hole spin. The case is markedly different at $V_b = -0.8$ V, in the uncharged regime. Here, the (negatively-polarized) X^- line is depolarized with a half-width, $B_{1/2} = 80$ G. With an estimated electron g-factor of $g_e = 0.2$ (*2*), $B_{1/2} = 80$ G corresponds to a time-averaged transverse spin lifetime $T_2^* = \hbar / B_{1/2} g_e \mu_B = 7$ ns, where μ_B is the Bohr magneton, and $\hbar$ is the Planck constant. This sharp Hanle peak has been previously attributed to the electron spin in the QD, prior to X^- formation (*2*). The X^0 line shows a much broader peak ($B_{1/2} = 4.1$ kG), with a small narrow component at low field. The broad component is consistent with the radiative lifetime of the exciton (~50 ps) (*4*). The narrow component has a half-width, $B_{1/2} = 95$ G, similar to the X^- width. In fact, this narrow peak is expected if a lone electron in the dot can bind and recombine with a subsequently injected hole. Similar features have been observed in ensemble Hanle measurements in GaAs QWs (*29*).

To summarize these PL results, in the uncharged regime spin-polarized excitons or electrons can be pumped into the dot. Both optical injection and trion recombination serve to pump spin-up electrons. At high bias in the charged regime ($V_b = 0.9$ V) the PL polarization is due to the hole spin, obscuring any information about the electron spin polarization. To address this issue, a more direct probe of the spin polarization is required.

To probe spins in the dot through KR, a second, linearly polarized, cw Ti:Sapphire laser is focused onto the sample, spatially overlapping the pump laser (*34*). The data in the top panel of Fig. 3A show the KR signal as a function of probe energy for σ^+ and σ^- pump helicity. Here, the applied bias is V_b = 0.2V and the QD is in the uncharged regime. The PL at this bias is also shown, with the X^- and X^0 energies indicated by the dotted lines. These energies coincide spectrally with two sharp features observed in the KR data, which we will refer to as Ξ^- and Ξ^0, respectively. In the bottom two panels of Fig. 3A the sum and difference of the σ^+ and σ^- data is shown. The feature Ξ^0 at the X^0 energy clearly does not depend on the sign of the injected spin and is similar to features seen in single dot absorption measurements (*17*). We attribute this peak to polarization-dependent absorption in the QD. We focus here on the (σ^+ - σ^-) data, which represents KR due to the optically oriented spin polarization. The feature Ξ^- at the X^- energy only appears in the difference data, indicating that it is due to the injected spin polarization, shown in Fig. 3B at four different bias voltages. For all voltages, the Ξ^- feature is centered at the X^- transition energy, indicated by the blue triangles. We can fit these data to Eq. 1 including only a single transition in the sum, on top of a broad background (red lines, Fig. 3B). From the free parameters in these fits we determine the transition energy E_0, amplitude A (defined as half the difference of the local maximum and minimum near E_0), and width Γ of the Ξ^- KR feature.

Figure 3D shows E_0 compared to the energy of the X^- PL line as a function of the applied bias. The two energies agree well and show the same quantum-confined Stark shift. Only at the highest bias, where significant broadening sets in, do we observe a small anti-Stokes shift between E_0 and the X^- PL energy. This may be caused by interactions with electrons in the QW. For a single electron spin in the QD ground state, the lowest energy optical transition contributing in Eq. 1 is the X^- transition (Fig. 3C). Thus the Ξ^- KR feature is due to the measurement of a single electron spin in the QD. We have repeated this measurement on another QD and observed the same Ξ^- feature, also at the X^- PL energy. The large, broad KR background is likely due to transitions involving excited electron and hole states, which are typically a few meV above the lowest transition (*18*).

If present, a KR feature due to the X^0 spin should appear centered at the XX transition energy. The signal-to-noise in our measurement is not high enough to conclusively identify such a feature. Despite the large amplitude of the X^0 PL compared to the X^- PL in the uncharged bias regime (~10:1), the short radiative lifetime of the X^0 state results in a low steady-state X^0 population, and therefore low KR signal.

By applying a transverse magnetic field B, we can monitor the depolarization of the single electron spin through the KR signal. In contrast to the Hanle measurements described above, the KR probes the spin in the QD directly and non-destructively, as opposed to being inferred from the spin-dependent formation of the X^-. The KR as a function of B is shown for three different bias voltages (Fig. 4A). At V_b = 0.2 V, in the uncharged regime, a narrow peak is observed with a half-width $B_{1/2}$ = 52 G, consistent with the X^- Hanle width measured in this regime. At V_b = 0.7 V, where the dot has charged, but the PL remains negatively polarized, we measure a somewhat wider KR depolarization curve, with $B_{1/2}$ = 150 G. When the QW is charged further, the spin lifetime decreases as shown at V_b = 1.1 V, with $B_{1/2}$ = 1.4 kG. Assuming an effective electron g-factor of 0.2 (*2*), these half-widths correspond to transverse spin lifetimes of 11, 3.3, and 0.8 ns, respectively.

The electron spin depolarization curves measured at probe energies detuned from the X^- transition by an energy, Δ, are shown in the top two panels of Fig. 4A for Δ = –0.3 meV (at the maximum of the Ξ^- feature), Δ = –2.7 meV (in the low energy tail), and Δ = +5.0 meV (on the broad, high energy feature). The curves have been normalized by their peak values, which vary with probe energy, but they show identical lineshapes for a given bias. This suggests that in this entire range of detuning, the KR of the same spin-polarized electron state in the QD is being probed.

Figure 4B shows $g_e T_2^* = \hbar / B_{1/2} \mu_B$ as a function of the applied bias, measured at a probe energy, E = 1.6288 eV, near the X^- transition. The dashed line indicates the onset of QD charging. The spin lifetime is largest in the uncharged regime. Here, $g_e T_2^*$ ~ 3 ns is consistent with previous measurements (*2*) in which the spin dephasing is attributed to the random, fluctuating hyperfine field (*30*, *31*). As the dot and well are charged, the electron spin lifetime decreases dramatically. This can be caused by the increasingly rapid capture of a second electron in the dot, which forms a spin-zero singlet state. Also, as discussed below, spin flips with electrons in the QW are likely to be a relevant mechanism in this regime.

The amplitude A of the Ξ^- KR signal is shown as a function of bias voltage (Fig. 4C). The amplitude decreases in the charged regime, reflecting the lower spin lifetime. We have argued above that spin-up electrons are pumped into the QD in the uncharged regime. Therefore the constant sign of the KR over the entire range of bias indicates spin-up polarization in the charged regime as well. Contrary to this observed polarization, the positively polarized X^- PL leaves a spin-down electron in the QD. However, this electron interacts with the bath of electrons in the QW, which is, on average, optically oriented in the spin-up direction. The predominant spin in the QW may be transferred to the electron in the dot via a higher order tunneling process (*32*). The finite spin-up polarization measured up to a large bias suggests that these electron-electron spin flips dominate over the X^--mediated spin pumping in the charged regime.

As the bias increases above V_b = 0.5V, the width of the Ξ^- KR feature, Γ, grows by a factor of 6, shown in Fig. 4D. A similar increase in linewidth is seen in the X^- PL in the charged regime. This provides further evidence for an increased coupling of the QD to other electronic states as the charging increases.

By probing a single electron in a QD through KR non-resonantly, we demonstrate a direct measurement of the electron spin with minimal perturbation to the system. As a first application, this method reveals information about spin dynamics in single QDs, and constitutes a pathway towards quantum non-demolition measurements and optically-mediated entanglement of single spins in the solid state. This scheme may also prove useful for non-destructive measurements in a variety of solid-state qubits, such as electrically-gated (*7*) or chemically-synthesized (*21*) QDs.

References and Notes

1. D. D. Awschalom, D. Loss, N. Samarth, Eds., *Semiconductor Spintronics and Quantum Computation* (Springer, Berlin, 2002).
2. A. S. Bracker *et al.*, *Phys. Rev. Lett.* **94**, 047402 (2005).
3. A. Ebbens *et al.*, *Phys. Rev. B* **72**, 073307 (2005).
4. T. H. Stievater *et al.*, *Appl. Phys. Lett.* **81**, 4251 (2002).
5. X. Li, Y. Wu, D. G. Steel, D. Gammon, L. J. Sham, *Phys. Rev. B* **70**, 195330 (2004).
6. A. Högele *et al.*, *Appl. Phys. Lett.* **86**, 221905 (2005).
7. J. M. Elzerman *et al.*, *Nature* **430**, 431 (2004).
8. J. M. Geremia, J. K. Stockton, H. Mabuchi, *Science* **304**, 270 (2004).
9. A. Kuzmich, L. Mandel, N. P. Bigelow, *Phys. Rev. Lett.* **85**, 1594 (2000).
10. F. Meier, D. D. Awschalom, *Phys. Rev. B* **70**, 205329 (2004).
11. B. Julsgaard, A. Kozhekin, E. S. Polzik, *Nature* **413**, 400 (2001).
12. M. N. Leuenberger, M. E. Flatté, D. D. Awschalom, *Phys. Rev. Lett.* **94**, 107401 (2005).
13. M. N. Leuenberger, *Phys. Rev. B* **73**, 075312 (2006).
14. D. V. Kupriyanov, I. M. Sokolov, *Quant. Opt.* **4**, 55 (1992).
15. F. Meier, D. D. Awschalom, *Phys. Rev. B* **71**, 205315 (2005).
16. J. R. Guest *et al.*, *Phys. Rev. B* **65**, 241310(R) (2002).
17. A. Zrenner *et al.*, *Phys. Rev. Lett.* **72**, 3382 (1994).
18. D. Gammon, E. S. Snow, B. V. Shanabrook, D. S. Katzer, D. Park, *Science* **273**, 87 (1996).
19. M. Sugita, S. Machida, Y. Yamamoto, http://arXiv.org/abs/quant-ph/0301064.
20. G. Salis, M. Moser, *Phys. Rev. B* **72**, 115325 (2005).
21. Y. Q. Li *et al.*, *Appl. Phys. Lett.* **88**, 193126 (2006).
22. R. J. Warburton *et al.*, *Nature* **405**, 926 (2000).
23. A. S. Bracker *et al.*, *Phys. Rev. B* **72**, 035332 (2005).
24. F. Meier, B. Zakharchenya, Eds., *Optical Orientation: Modern Problems in Condensed Matter Sciences, Vol. 8* (North Holland, Amsterdam, 1984).
25. R. I. Dzhioev *et al.*, *Phys. Solid State* **40**, 1587 (1998).
26. S. Cortez *et al.*, *Phys. Rev. Lett.* **89**, 207401 (2002).
27. J. G. Tischler, A. S. Bracker, D. Gammon, D. Park, *Phys. Rev. B* **66**, 081310(R) (2002).
28. Y. El Khalifi, B. Gil, H. Mathieu, T. Fukunaga, H. Nakashima, *Phys. Rev. B* **39**, 13533 (1989).
29. R. I. Dzhioev *et al.*, *Phys. Rev. B* **66**, 153409 (2002).
30. A. V. Khaetskii, D. Loss, L. Glazman, *Phys. Rev. Lett.* **88**, 186802 (2002).
31. I. A. Merkulov, Al. L. Efros, M. Rosen, *Phys. Rev. B* **65**, 205309 (2002).
32. J. Lehmann, D. Loss, *Phys. Rev. B* **73**, 045328 (2006).
33. We thank Y. K. Kato for useful advice and discussions and acknowledge support from NSF and AFOSR.
34. Materials and methods are available as supporting material on *Science* Online.

Supporting Online Material
www.sciencemag.org/cgi/content/full/1133862/DC1
Materials and Methods
References

14 August 2006; accepted 1 November 2006
Published online 9 November 2006;
10.1126/science.1133862
Include this information when citing this paper.

Fig. 1. Sample structure and characterization. (**A**) Schematic of the sample structure. (**B**) The calculated conduction (valence) band profile shown in solid (dashed) lines. Raising the bias voltage from $V_b = -1$ V to 1 V, the QW conduction band minimum is lowered past the Fermi level (blue). (**C**) The calculated electron density, *n*, in the QW showing the onset of charging at $V_b = 0.5$ V. (**D**) The reflectivity, *R*, of the cavity at T = 10 K, with a resonance at 763.6 nm.

Fig. 2. Single dot PL and Hanle measurements. (**A**) PL of a single QD as a function of bias voltage. A jump in the PL energy indicates the onset of QD charging. (**B**) The polarization of the X^- and X^0 PL lines as a function of bias. (**C**) Hanle curves in the charged regime (blue), and in the uncharged regime (black and red).

Fig. 3. Single dot KR spectra. (**A**) Top panel: KR measured with σ^+ and σ^- polarized pump at $V_b = 0.2$ V. The PL at this bias is also shown. Middle panel: the sum of the σ^+ and σ^- data showing a spin-independent feature Ξ^0 at the X^0 energy. Bottom panel: The difference of the σ^+ and σ^- data with the feature Ξ^- at the X^- energy circled. (**B**) Single spin KR (Ξ^-) at various bias voltages. The blue triangle indicates the energy of the X^- PL line. Fits to the data are shown in red. (**C**) Illustration of three relevant optical transitions. (**D**) The agreement between the X^- PL energy and the Ξ^- energy. The biexciton PL energy is also shown for comparison.

Fig. 4. KR depolarization and analysis. (**A**) KR as a function of transverse magnetic field for various bias voltages. The top two panels show measurements with the probe at various detunings, Δ, from the X^- energy. (**B**) $g_eT_2^*$ determined from the KR half-width. The red triangle indicates the value obtained form the Hanle measurement. (**C** and **D**) The amplitude and width of the KR Ξ^- feature as a function of applied bias.

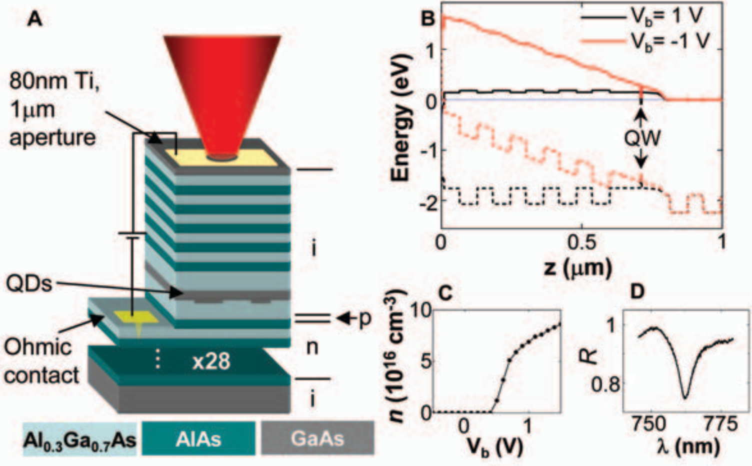
A
80nm Ti,
1μm
aperture
QDs
Ohmic
contact
x28
i
p
n
i
Al0.3Ga0.7As
AlAs
GaAs
B
V_b= 1 V
V_b= -1 V
Energy (eV)
1
0
-1
-2
QW
0
0.5
1
z (μm)
C
n (10^16 cm^-3)
10
5
0
0
1
V_b (V)
D
R
1
0.8
750
775
λ (nm)

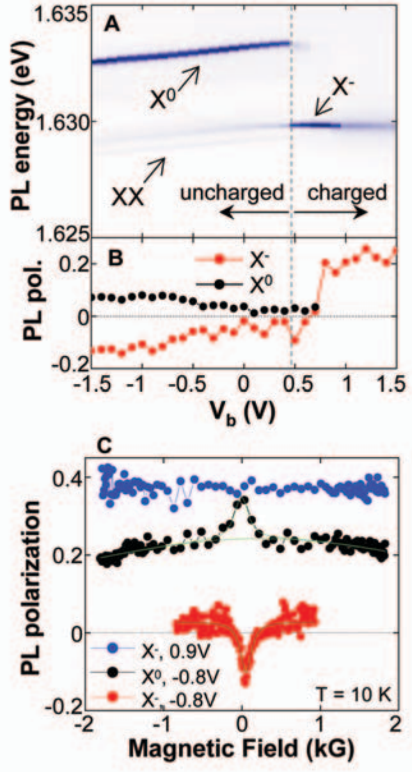

A
PL energy (eV)
1.635
1.630
1.625
X⁰
X⁻
XX
uncharged
charged
B
PL pol.
X⁻
X⁰
0.2
0
-0.2
-1.5
-1
-0.5
0
0.5
1
1.5
V_b (V)
C
PL polarization
0.4
0.2
0
-0.2
X⁻, 0.9V
X⁰, -0.8V
X⁻, -0.8V
T = 10 K
-2
-1
0
1
2
Magnetic Field (kG)

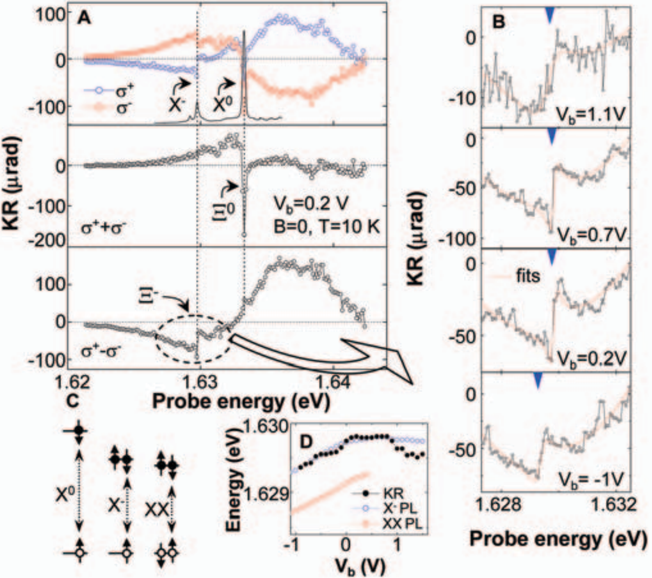
A
B
C
D
KR (μrad)
Probe energy (eV)
σ+
σ-
X-
X0
Ξ0
Ξ-
σ++σ-
σ+-σ-
Vb=0.2 V
B=0, T=10 K
100
0
-100
-200
1.62
1.63
1.64
Vb=1.1V
Vb=0.7V
Vb=0.2V
Vb= -1V
fits
-10
-50
1.628
1.632
X0
X-
XX
Energy (eV)
1.630
1.629
Vb (V)
-1
0
1
KR
X- PL
XX PL

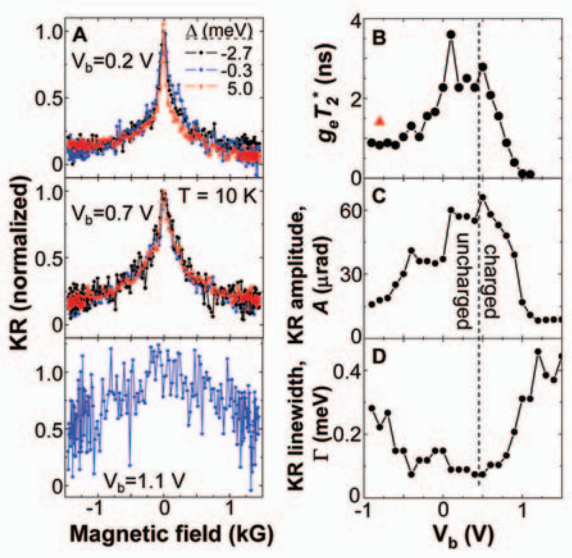
A
Δ (meV)
-2.7
-0.3
5.0
V_b=0.2 V
T = 10 K
V_b=0.7 V
V_b=1.1 V
KR (normalized)
1.0
0.5
0
-1
0
1
Magnetic field (kG)
B
$g_e T_2^*$ (ns)
4
2
0
C
KR amplitude, A (μrad)
60
30
0
uncharged
charged
D
KR linewidth, Γ (meV)
0.4
0.2
0
-1
0
1
V_b (V)